Ambient catalyst-free nitrogen fixation with water dimer radical cation

Xiaoping Zhang[a], Rui Su[b], Jingling Li[a], Liping Huang[c], Wenwen Yang[a], Konstantin Chingin[b], Roman Balabin[b], Jingjing Wang[b], Xinglei Zhang[a], Weifeng Zhu[c], Keke Huang[b], Shouhua Feng*[b], Huanwen Chen*[a,c]

[a] Prof. X. Zhang, J. Li, W. Yang, Prof. X. Zhang, Prof. H. Chen
Jiangxi Key Laboratory for Mass Spectrometry and Instrumentation, East China University of Technology
Nanchang, 330013, P. R. China
E-mail: chw8868@gmail.com

[b] Prof. R. Su, Prof. K. Huang, Prof. S. Feng
State Key Laboratory of Inorganic Synthesis and Preparative Chemistry, College of Chemistry, Jilin University
Changchun 130012, P. R. China

[c] Prof. L. Huang, Prof. K. Chingin, Prof. R. Balabin, J. Wang, Prof. W. Zhu, Prof. H. Chen
School of Pharmacy, Jiangxi University of Chinese Medicine
Nanchang, 330004, P. R. China

Supporting information for this article is given via a link at the end of the document.

Abstract: The growth and sustainable development of humanity is heavily dependent upon the process of fixing nitrogen (N_2) to ammonia (NH_3). However, the currently adopted methods are associated with severe environmental hazards and tremendous energy costs, which limit their sustainability and profitability. Herein we discovered a catalyst-free disproportionation reaction of N_2 by water dimer radical cation, $(H_2O)_2^{+\bullet}$, which occurs under mild ambient conditions *via* distinctive HONH-HNOH$^{+\bullet}$ intermediate to yield economically valuable nitroxyl (HNO) and hydroxylamine (NH_2OH) products, in alternative to NH_3. Calculations suggest that the reaction is prompted by the coordination of electronically excited N_2 with $(H_2O)_2^{+\bullet}$ in its two-center-three-electron (2c-3e) configuration. Subsequent excited-state double proton transfer leads to one-step water addition to N_2. The ambient fixation of N_2 into HNO and NH_2OH with high selectivity offers great profitability and total avoidance of polluting emissions, such as CO_2 or NO_y, thus giving an entirely new look and perspectives to the problem of green N_2 fixation.

Introduction

Nitrogen is an essential element for all living organisms on our planet. Molecular nitrogen (N_2) accounts for more than 99% of global nitrogen [1] but is extremely chemically stable and thus cannot be directly utilized unless fixed by alternating its oxidation state into bioavailable forms [2]. Since the advent of energy-intensive Haber-Bosch (HB) process early in the 20th century and up to the present time, N_2 on Earth has been predominantly fixed in the form of ammonia (NH_3), which has largely shaped our world and its heavy dependence on NH_3 [3]. However, the intensive reaction conditions (ca. 100 bar and 500°C), severe environmental pollution (>1% of the global carbon emission) and high consumption of fossil fuel (1%–2% of global energy consumption) in the HB process are becoming increasingly crucial for the global sustainable development and urge novel strategies for N_2 fixation under mild conditions [4]. Extensive research is being done in search of alternative strategies for N_2 fixation to NH_3, including electrocatalytic [5], photocatalytic [6], biological [7], and plasma-based [8] methods, but none of these methods have yet been able to rival the overall performance of HB process with regard to the cost efficiency, scalability and selectivity of NH_3 production [5a, 9].

In parallel, it is also of paramount interest to explore alternative molecular mechanisms of fixing N_2 that would obviate the production of NH_3 and thus alleviate the current dependence of society on NH_3 [3, 10]. The global production and utilization of NH_3 are associated with a great number of critical issues, including its severe environmental implications, toxicity, flammability, explosion hazards, corrosiveness, difficulties of transportation and storage, etc, which are increasingly at odds with the paradigm of sustainable development [3]. In fact, the prodigious amounts of NH_3 utilized on Earth at present time are to a larger degree dictated by the scarcity of alternative routes of N_2 fixation rather than by the intrinsic usability of NH_3. Up to date, several catalytic systems have been demonstrated to have a potential of activating the super-strong N≡N triple bond, however their practical applications are yet to be explored [10c, 11]. N_2 fixation into NH_3 and NO_y (NO, NO_2, NO_3, HNO_3, HNO_2, *etc*) has been reported in several plasma-based methods [8, 9b, 12]. However, NO_y are toxic to the environment. Also, the production of NH_3 and NO_y in plasma-based methods currently comes at the cost of N_2 dissociation/burning and therefore poor chemical selectivity and high energy costs [8, 9b].

Recent studies indicate that the N≡N bond can be weakened by accepting electrons from the bonding orbitals of N_2 to the antibonding orbitals and/or donating electrons, which would make its functionalization feasible [13]. The weakening of N≡N bond could be further promoted through the excitation of N_2 into its triplet state, *e.g.*, by electronic or collisional activation [14]. Recently, we have discovered that abundant radical cations of water clusters, especially in the dimer form, $(H_2O)_2^{+\bullet}$, can be produced by depositing suitable amounts of energy into the pure water vapor at atmospheric pressure [15]. The as-prepared water radical cations showed the high reactivity toward a wide range of volatile

molecules, such as benzene, acetone, ethyl acetate and dimethyl disulphide, revealing rich chemistry with the ionic and radical characters [15-16]. Here we discovered that, owing to its distinct 2c-3e configuration, $(H_2O)_2^{+\bullet}$ can specifically activate N_2 via the formation of $HONH\text{-}HNOH^{+\bullet}$ intermediate to selectively disproportionate it into hydroxylamine (NH_2OH) and nitroxyl (HNO) products under mild ambient conditions and with no catalyst involved.

Results and Discussion

Disproportionation reaction of N_2 with $(H_2O)_2^{+\bullet}$

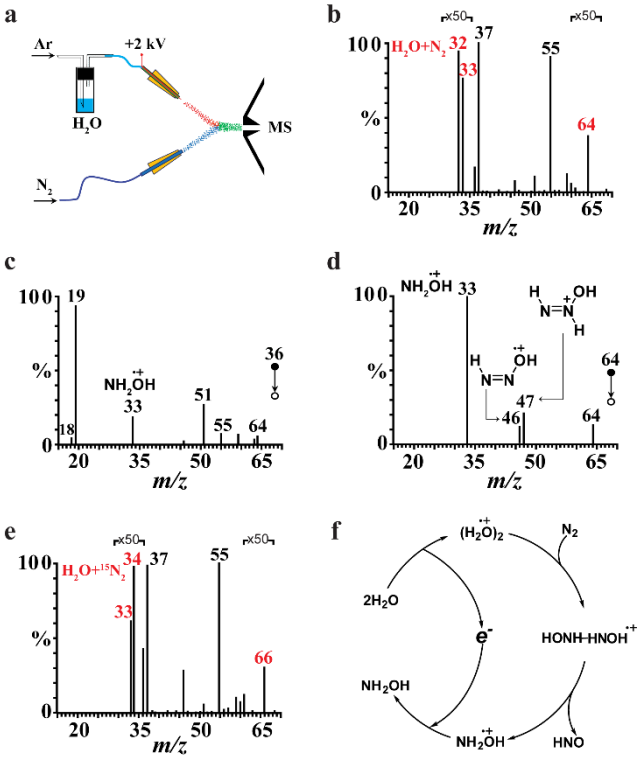

Figure 1. Ambient disproportionation reaction of N_2 with water dimer radical cation. (a) Experimental setup to study the interaction of N_2 with water vapor plasma by online mass spectrometry. (b) Mass spectrum of the ionic species. Red-color marks correspond to the products specific to the reaction between water vapor plasma and N_2. (c) Mass spectrum of ionic products for the gas-phase reaction between N_2 and isolated $(H_2O)_2^{+\bullet}$ (*m/z* 36) in the ion trap. (d) Ionic fragments of the reaction intermediate at *m/z* 64. (e) Mass spectrum of the ionic species observed during the interaction between water vapor plasma and $^{15}N_2$ ($^{15}N_2$ gas instead of $^{14}N_2$ in a). Red-color marks correspond to the products specific to the reaction between water vapor plasma and $^{15}N_2$. (f) Schematic diagram summarizing a possible mechanism for the reaction of N_2 with $(H_2O)_2^{+\bullet}$.

In our first experiment, water plasma was generated by discharge of water/argon vapor mixture (Figure S1a). The major ionic species observed by real-time mass spectrometry detection included protonated water clusters, $(H_2O)_2H^+$ (*m/z* 37) and $(H_2O)_3H^+$ (*m/z* 55), as well as abundant water dimer radical cation, $(H_2O)_2^{+\bullet}$ (*m/z* 36) (Figure S1b), in agreement with previous reports [15-17]. Remarkably, when N_2 was introduced to intersect with the water plasma (Figure 1a) or when the carrier gas (Ar) in the ion source was replaced by N_2, abundant ions of *m/z* 32 and *m/z* 33 and *m/z* 64 were additionally observed (Figure 1b). We tentatively assigned these signals to $HNOH^+$ (*m/z* 32), $NH_2OH^{+\bullet}$ (*m/z* 33) and $HONH\text{-}HNOH^{+\bullet}$ (*m/z* 64), respectively. We speculated that these new ionic species could be derived through the reaction between $(H_2O)_2^{+\bullet}$ and N_2. To verify this assumption, $(H_2O)_2^{+\bullet}$ ions (*m/z* 36) were isolated and activated in the ion trap by RF field (~ 100 $V_{p\text{-}p}$) in the presence of neutral N_2 gas, which was directly introduced into the ion trap. As the result, the product signals were unambiguously observed at *m/z* 18 (elimination of H_2O from $(H_2O)_2^{+\bullet}$), *m/z* 19 (elimination of $^{\bullet}OH$ from $(H_2O)_2^{+\bullet}$), *m/z* 33 ($NH_2OH^{+\bullet}$), *m/z* 51 ($NH_2OH^{+\bullet}$ plus H_2O), *m/z* 55 ($(H_2O)_3H^+$) and *m/z* 64 ($HONH\text{-}HNOH^{+\bullet}$) (Figure 1c). Curiously, the signal of $HNOH^+$ abundantly produced upon the interaction between water plasma and N_2 (*m/z* 32 in Figure 1b) was almost undetectable when $(H_2O)_2^{+\bullet}$ was activated in the ion trap (Figure 1c), probably because the HNO was initially created as neutral species. During the interaction between water plasma and N_2, neutral HNO could be easily protonated by other ionic species such as $(H_2O)_2H^+$ (*m/z* 37) to give the protonated signal at *m/z* 32 (Figure 1b), whereas when produced in the ion trap neutral HNO would be instantly pumped out of the ion trap (maintained at high vacuum of 10^{-5} Torr).

The signal at *m/z* 64 was assigned to $HONH\text{-}HNOH^{+\bullet}$ intermediate produced during the reaction between N_2 and $(H_2O)_2^{+\bullet}$ inside the ion trap. The chemical assignment of the *m/z* 64 signal to $HONH\text{-}HNOH^{+\bullet}$ was supported by collision-induced dissociation (CID) data (Figure 1d), showing the characteristic fragment at *m/z* 33 corresponding to the elimination of HNO, accompanied by lower-intensity fragments at *m/z* 46 and *m/z* 47 (also discerned in the spectra Figure 1b, c), corresponding to the elimination of H_2O and $^{\bullet}OH$ (the dissociation path shown in Figure S1c), respectively. These chemical assignments were further supported by experiments with isotopic substituents (Figure 1e, Figure S1d, S1e). When H_2O in our experiments was replaced by deuterated water, D_2O, the abundant signals at *m/z* 33, *m/z* 34 and *m/z* 35 (Figure S1d) were observed, indicating the formation of $HNOD^+$, $DNOD^+/NH_2OD^{+\bullet}$, and $NHDOD^{+\bullet}$, respectively. Similarly, when N_2 was replaced by $^{15}N_2$, the signals at *m/z* 33 and *m/z* 34 were detected (Figure 1e), indicating the formation of $H^{15}NOH^+$ and $^{15}NH_2OH^{+\bullet}$, respectively. Interestingly, the $HONH\text{-}HNOH^{+\bullet}$-type intermediate was also detected in the experiments with isotopic substitutes: as $DOND\text{-}DNOD^{+\bullet}$ (*m/z* 68) for the D_2O experiment (Figure S1d) and as $HO^{15}NH\text{-}H^{15}NOH^{+\bullet}$ (*m/z* 66) for the $^{15}N_2$ experiment (Figure 1e), respectively. Note that the intermediates labelled with different isotopes showed the identical fragmentation path (Figure S1e). Further reference experiments carried out in our lab indicated that the observed nitrogen disproportionation occurred specifically as the result of reaction between neutral N_2 and water radical cations: no products could be detected when isolated $N_2^{+\bullet}$ was exposed to neutral water vapor in the ion trap (Figure S1f). Therefore, the spectral data obtained in all the above-mentioned experiments strongly indicate that the observed species correspond to the disproportionation reaction of N_2 with $(H_2O)_2^{+\bullet}$.

Detailed experimental conditions are provided in the Supporting Information. Figure 1a displays the experimental setup. Briefly, substrate water solutions are forced using a syringe pump through

a fused silica capillary that sits inside a larger coaxial capillary through which high-pressure N2 sheath gas flows. Figure 1b shows a typical mass spectrum showing the spontaneous generation of $(H_2O)_2^+$ at m/z 36 when pure water is sprayed to form microdroplets.

Derived from the experimental observations and theoretical calculations, a possible reaction pathway for N_2 disproportionation with $(H_2O)_2^{+\bullet}$ is proposed as shown in Figure 1f and Figure 2. First, neutral H_2O is ionized to form $(H_2O)_2^{+\bullet}$ species [15-16]. Our calculations indicate that N_2 disproportionation with $(H_2O)_2^{+\bullet}$ is thermodynamically not allowed ($\Delta E \approx 4.0$ eV) when N_2 is present in its ground singlet ($X\ ^1\Sigma_g^+$) state (Figure S2) but may occur ($\Delta E \approx -3.8$ eV) when N_2 is present in its more active triplet ($A\ ^3\Sigma_u^+$) state, N_2* (Figure 2). It is well known that N_2 is effectively transferred from its singlet state to its triplet state through the collisions with electrons (*e.g.*, in N_2 and CO_2 gas lasers), ions or molecules [14a]. It has been shown that, owing to its high molecular symmetry, N_2* exhibits unique stability and lives for up to 1.3 s [18], which allows its involvement in chemical reactions, such as the above-mentioned N_2 disproportionation. In our experiments singlet N_2 could be activated to triplet N_2* through collisions: with high-energy charged species in the ion source (Figure 1a, b) or with accelerated $(H_2O)_2^{+\bullet}$ species in the ion trap (Figure 1c). Our calculations indicate that out of the two co-existing $(H_2O)_2^{+\bullet}$ structures, *i.e.*, hydrogen-bonded $[H_3O^+\bullet\bullet\bullet OH]$ and two-center-three-electron (2c-3e) $[H_2O\bullet\bullet\bullet OH_2]^+$[15], the latter could effectively react with N_2* (Figure 2).

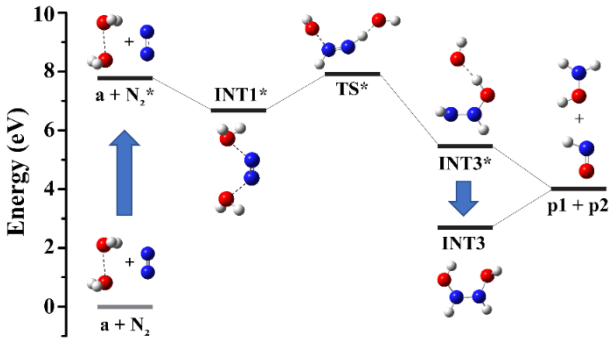

Figure 2. The geometries and electronic energies of possible molecular and ionic species involved in the disproportionation reaction $N_2 + (H_2O)_2^{+\bullet} \rightarrow NH_2OH^{+\bullet} + HNO$ calculated with B2GP-PLYP density functional. Vertical arrow corresponds to electronic excitation of N_2. a: $[H_2O\bullet\bullet\bullet OH_2]^+$. p1: $NH_2OH^{+\bullet}$. p2: HNO.

The association of $[H_2O\bullet\bullet\bullet OH_2]^+$ structure with N_2* occurs due to stabilization of the positive charge jointly by the N_2 and the two H_2O moieties (INT1*, Figure 2). The INT1* structure is then converted into the excited-state intermediate HONH-HNOH$^{+\bullet}$* (INT3*, $\Delta E = -1.2$ eV, Figure 2) by the direct double-proton transfer through TS* structure (Figure 2). The HONH-HNOH$^{+\bullet}$* intermediate spontaneously and irreversibly dissociates into neutral HNO and cationic $NH_2OH^{+\bullet}$ ($\Delta E = -1.5$ eV, Figure 2). In addition to the dissociation channel, HONH-HNOH$^{+\bullet}$* could also relax to its ground state, HONH-HNOH$^{+\bullet}$ (INT3, $\Delta E = -2.8$ eV, Figure 2), without dissociation. It is probably through this latter channel that the stable HONH-HNOH$^{+\bullet}$ signal is detected in our experiments (*m/z* 64, Figure 1). The HONH-HNOH$^{+\bullet}$ structure could dissociate into HNO and $NH_2OH^{+\bullet}$ by collisional activation ($\Delta E = 1.3$ eV, Figure 2), just as observed in the ion trap experiments (Figure 1d). The $NH_2OH^{+\bullet}$ product can be neutralized to NH_2OH by electron transfer from the environment.

Overall, it is clear that N_2 fixation by $(H_2O)_2^{+\bullet}$ *via* HONH-HNOH$^{+\bullet}$ intermediate is mechanistically distinct from the earlier described processes of catalytic nitrogen fixation at a heterogeneous surface [19], in which nitrogen reduction on metal catalyst usually proceeds *via* N_2H_x-type intermediates ($0 \le x \le 2$). Therefore, this report presents a new mechanism of N_2 fixation.

Scale-up reaction

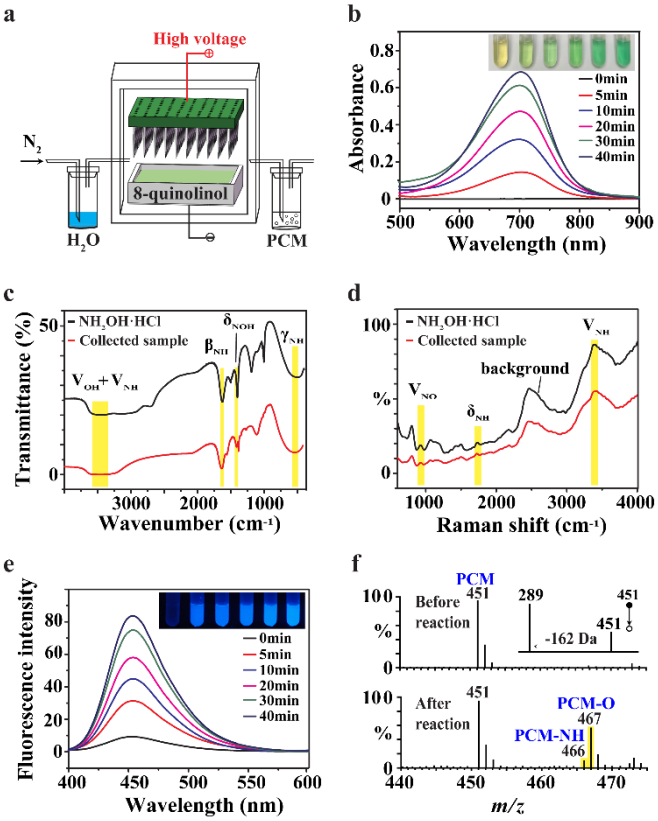

Figure 3. Products of ambient disproportionation reaction of N_2 with $(H_2O)_2^{+\bullet}$ characterized by spectral methods. (a) Schematic illustration of the reaction assembly for scale-up reaction and the collection of reaction products. (b) UV-Vis spectra of indooxine formed through the online reaction of the collected NH_2OH with 8-quinolinol probe at different times of the reaction between N_2 and $(H_2O)_2^{+\bullet}$. (c) Infrared spectra of the collected sample (red) and NH_2OH•HCl standard (black). (d) Raman spectra of the collected sample (red) and NH_2OH•HCl standard (black). (e) Fluorescence spectra of 7-hydroxycoumarin formed through the online reaction of the collected HNO with PCM probe at different times of the reaction between N_2 and $(H_2O)_2^{+\bullet}$. (f) Mass spectra of PCM solution before and after collection of the reaction mixture, showing the formation of PCM aza-ylide (PCM-NH) and PCM oxide (PCM-O) due to the reaction between PCM and HNO. The inset figure shows the tandem mass spectrum of protonated PCM at *m/z* 451.

The disproportionation reaction of N_2 with $(H_2O)_2^{+\bullet}$ was scaled up under ambient conditions using the setup in Figure 3a, which consisted of an array of 76 needles evenly distributed on a ~ 3.5 × 5.5 cm^2 tungsten plate to generate abundant $(H_2O)_2^{+\bullet}$ and the accessories to collect the NH_2OH and HNO products. We found that NH_2OH was most efficiently collected at the cathode electrode, while HNO was most efficiently collected through the neutral outlet line (Figure 3a). These observations further support the conclusion that NH_2OH in the reaction was formed in cationic form while HNO was formed in neutral form.

Under the optimized experimental conditions (Figure S3), the production of 18.5μM NH_2OH and 17.7 μM HNO products could be achieved within just 10 min, as quantified by standard spectrophotometric methods (Figure S4). The collected NH_2OH was reacted with an optical probe 8-quinolinol to form indooxine, which was quantified by UV-Vis spectroscopy [20]. The signal intensity showed clear correlation with the time of the reaction between N_2 and $(H_2O)_2^{+\bullet}$ (Figure 3b). The formation of indooxine due to the reaction between NH_2OH and 8-quinolinol was further confirmed by tandem MS experiments through the comparison with indooxine standard (Figure S5a). The formation of NH_2OH product due to the disproportionation reaction between N_2 and $(H_2O)_2^{+\bullet}$ was further validated by infrared (Figure 3c) and Raman (Figure 3d) spectroscopy of the collected samples.

Similarly, the collected HNO was reacted with a coumarin-based fluorescent probe PCM to form 7-hydroxycoumarin. The 7-hydroxycoumarin was quantified by fluorescence spectroscopy. The signal intensity showed clear correlation with the time of the reaction between N_2 and $(H_2O)_2^{+\bullet}$ (Figure 3e). The occurrence of the reaction between PCM and the HNO product was further confirmed by the detection of other products of the reaction between PCM and HNO: the PCM aza-ylide and PCM oxide (Figure 3f, Figure S5b), which were in good agreement with the literature data [21]. Note that the preparation and characterization of PCM is described in Figures S5c, S5d.

Reference experiments performed using the scaled-up setup shown in Figure 3a when N_2 was replaced by Ar showed the total absence of characteristic NH_2OH and HNO signals in the collected samples, thus indicating that the NH_2OH and HNO products were generated specifically due to the reaction of $(H_2O)_2^{+\bullet}$ with N_2 (Figure S6). Therefore, the reference measurements and the mass spectrometry, vibrational spectroscopy and optical spectroscopy data altogether provide unambiguous proofs for the formation of NH_2OH and HNO in the disproportionation reaction between N_2 and water radical cations $(H_2O)_2^{+\bullet}$.

conversion rate of almost 100% within ca. 30 min (Figure 4b). The simplicity of the experimental assembly suggests that the disproportionation reaction between N_2 and $(H_2O)_2^{+\bullet}$ could probably serve the agricultural fields as tiny onsite ammonia plants, which could be powered by solar cells [27].

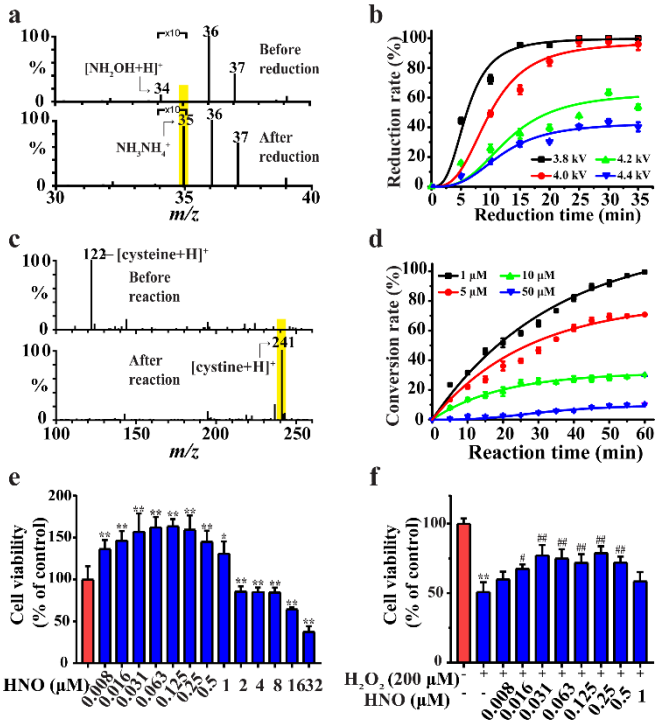

Figure 4. Further validation and application of the NH_2OH and HNO products of N_2 disproportionation with $(H_2O)_2^{+\bullet}$. (a) Electrolytic reduction of the collected NH_2OH product (corresponding signal at *m/z* 34) into NH_3 (corresponding signal at *m/z* 35) confirmed by MS detection. The signals at *m/z* 36 and *m/z* 37 correspond to $(H_2O)_2^{+\bullet}$ and $H^+(H_2O)_2$. (b) The kinetics of electrolytic reduction of NH_2OH collected at different discharge voltages into NH_3 determined using the indophenol blue method (45) (Figure S7). (c) The conversion of cysteine (corresponding signal at *m/z* 122) into cystine (corresponding signal at *m/z* 241) via the reaction of cysteine with the collected HNO product of the disproportionation reaction of N_2 confirmed by MS detection. (d) The kinetics of cysteine conversion into cystine via the reaction with the collected HNO product (~25 μM; collection time 30 min) at different cysteine concentrations. (e) Effects of different concentration levels of HNO alone on HT22 cell viability. (f) HT22 cells were pretreated with different concentration levels of HNO for 24 h and incubated with or without H_2O_2 (200 μM) for 1 h. Cell viability as determined with CCK-8 assay. $^{*}P<0.05$ and $^{**}P<0.01$versus control, $^{\#}P < 0.05$ and $^{\#\#}P < 0.01$ versus model.

Application of the reaction products

Note that the both products of the disproportionation reaction between N_2 and $(H_2O)_2^{+\bullet}$ are highly valuable chemicals. For example, NH_2OH is widely used as an important chemical raw material, *e.g.* to prepare oximes [22], anilines [23], amides [24], and sulfonamides [25], as well as energetic fuel for space rockets [26]. Further, using a low-cost homemade setup powered by a 1.5 V solar cell battery (Figure S7a) in our laboratory, we were able to easily reduce the prepared NH_2OH into NH_3 (Figure 4a) with the

The other reaction product, HNO (as the active ingredient of medicine such as Angeli's salt (AS) [28], is a currently expensive material for medical and biology utilities [29], particularly for biological targets of thiols and metalloproteins in fighting cancer [30]. Further, here we also showed that the HNO product of the reaction between N_2 and $(H_2O)_2^{+\bullet}$ could be used to directly convert cysteine into cystine (Figure 4c) with the conversion rate of almost 100% within ca. 60 min (Figure 4d) under the conditions tested, suggesting that HNO could be used for the specific chemical modification of thiols in proteins, which is consistent with previous

report of authentic AS [28]. These data further validate the formation of NH_2OH and HNO during the reaction between N_2 and $(H_2O)_2^{+\bullet}$ and demonstrate the potential applications of these products.

Importantly, HNO is known for its cardioprotective and neuroprotective effects [29]. In addition, HNO is resistant to superoxide scavenging and tolerance development [31]. Here we investigated whether the HNO product of disproportionation reaction could be used for protection against neurotoxicity. Figure 4e shows the effect of HNO concentration levels on the viability of HT22 cells. The results indicate that the application of HNO in the range from 0.008 μM to 1 μM poses no cytotoxic effect on the HT22 cells and promotes their proliferation. The EC50 and IC50 were estimated as 0.016 μM and 18.12 μM, respectively (Figure S8a, b). The viability of HT22 cells was greatly reduced when exposed to exogenous source of free radicals, H_2O_2 at 200 μM (~50%, $P < 0.01$ vs. the control group) (Figure 4f, Figure S8c, d). Remarkably, HT22 cells incubated with HNO displayed significantly higher resistance to the H_2O_2-induced damage, with maximum protection at 0.25 μM concentration of HNO (79%, $P < 0.01$ vs. the 2 group) (Figure 4f). The results of our cell viability assay indicate that the HNO product could be used to protect HT22 cells against H_2O_2-induced damage. As the research continues in this field, it is likely that further novel properties, endogenous actions and therapeutic applications of HNO will be discovered.

Characteristics of the N_2 disproportionation reaction

Using the total plate area (~ 3.5 × 5.5 cm^2) as the active area of the 76-pin device (Figure 3a), we estimated the Faradic efficiency (FE) ≈ 64% with the yield ≈ 1.14 μg cm^{-2} h^{-1} for NH_2OH and the FE ≈ 20% with the yield ≈ 0.37 μg cm^{-2} h^{-1} for HNO (optimized in Figure S9). Note that the maximum yields calculated based only on the total effective surface area of 76 needle tips were 5.10 ×10^3 μg cm^{-2} h^{-1} for NH_2OH and 1.53×10^3 μg cm^{-2} h^{-1} for HNO, respectively, since only the tip surface of the needles were activated for the N_2 disproportionation reaction (see detailed footnotes in Table S1). The lower yield and FE for HNO is probably caused by its higher reactivity, resulting in the partial conversion of HNO by H_2O and other chemicals in the collecting solution. Compared to the majority of previously reported approaches for nitrogen reduction under mild conditions (Table S1) [32], including plasma methods (Table S2), our method provides reasonably high efficiency and yield. Other key merits of our method include: 1) mild conditions; total avoidance of toxic reagents and by-products; low cost; easy implementation; scalability; 2) low energy consumption, high efficiency and high-value products: according to the current market, the potential value about 1.5 $ of NH_2OH and 7310 $ of HNO (as derived from the AS application) were produced by 1 kWh of electricity (≤ 0.2 $); 3) no chemical catalyst needed; 4) high atom economy: the oxidation of one nitrogen atom of N_2 to HNO coupled with the simultaneous reduction of the other nitrogen atom of N_2 to NH_2OH.

Conclusion

In summary, we have demonstrated that the atmospheric N_2 can be disproportionately fixed by $(H_2O)_2^{+\bullet}$ under ambient conditions into economically valuable NH_2OH and HNO, presenting an alternative to the current necessity of fixing N_2 into NH_3. The combination of the essential N, O and H atoms in the obtained products considerably increases variability of possible chemistries as compared to NH_3 [23, 33]. The experimental and theoretical studies indicate that triplet-state N_2 is activated by $(H_2O)_2^{+\bullet}$ to form intermediate HONH-$HNOH^{+\bullet}$, which is further decomposed to form $NH_2OH^{+\bullet}$ and HNO. The mechanism of N_2 fixation by the 2c-3e $(H_2O)_2^{+\bullet}$ structure through the excited-state double-proton transfer is principally different from the previously proposed methods. The design ideas in this work could motivate more research efforts to further explore the potential of distinct $(H_2O)_2^{+\bullet}$ chemistry and open new possibilities for green nitrogen fixation.

Acknowledgements

The authors acknowledge Dr. Lili Sun for preliminary calculations. The authors also thank Ms. Xuejiao Chen and Mr. Yuan Zhong for their help in designing the MS experiments. The authors are particularly grateful for the proof reading of the manuscript by Prof. Yinquan Wang. The work was supported by National Natural Science Foundation of China (No.21520102007, 22104014).

Keywords: Nitrogen fixation • water radical cation • disproportionation reaction • ambient • two-center-three-electron

[1] L. Y. Yeung, S. Li, I. E. Kohl, J. A. Haslun, N. E. Ostrom, H. Hu, T. P. Fischer, E. A. Schauble, E. D. Young, *Sci. Adv.* **2017**, *3*, 6741.

[2] M. A. Legare, G. Belanger-Chabot, R. D. Dewhurst, E. Welz, I. Krummenacher, B. Engels, H. Braunschweig, *Science* **2018**, *359*, 896-899.

[3] J. W. Erisman, M. A. Sutton, J. Galloway, Z. Klimont, W. Winiwarter, *Nat. Geosci.* **2008**, *1*, 636-639.

[4] a) J. G. Chen, R. M. Crooks, L. C. Seefeldt, K. L. Bren, R. M. Bullock, M. Y. Darensbourg, P. L. Holland, B. Hoffman, M. J. Janik, A. K. Jones, M. G. Kanatzidis, P. King, K. M. Lancaster, S. V. Lymar, P. Pfromm, W. F. Schneider, R. R. Schrock, *Science* **2018**, *360*, aar6611; b) Y. Tanabe, Y. Nishibayashi, *Chem. Soc. Rev.* **2021**, *50*, 5201-5242.

[5] a) J. Li, X. Guo, L. Gan, Z.-F. Huang, L. Pan, C. Shi, X. Zhang, G. Yang, J.-J. Zou, *ACS Appl. Energy Mater.* **2022**, *5*, 9241-9265; b) Y. Fang, Y. Xue, Y. Li, H. Yu, L. Hui, Y. Liu, C. Xing, C. Zhang, D. Zhang, Z. Wang, X. Chen, Y. Gao, B. Huang, Y. Li, *Angew. Chem. Int. Ed.* **2020**, *59*, 13021-13027.

[6] M.-H. Vu, M. Sakar, S. A. Hassanzadeh-Tabrizi, T.-O. Do, *Adv. Mater. Interfaces* **2019**, *6*, 1900091.

[7] A. Soumare, A. G. Diedhiou, M. Thuita, M. Hafidi, Y. Ouhdouch, S. Gopalakrishnan, L. Kouisni, *Plants* **2020**, *9*, 1011.

[8] L. R. Winter, J. G. Chen, *Joule* **2021**, *5*, 300-315.

[9] a) A. J. Martín, T. Shinagawa, J. Pérez-Ramírez, *Chem* **2019**, *5*, 263-283; b) Z. Huang, A. Xiao, D. Liu, X. Lu, K. Ostrikov, *Plasma Process. Polym.* **2022**, *19*, 2100198.

[10] a) J. W. Erisman, J. N. Galloway, S. Seitzinger, A. Bleeker, N. B. Dise, A. M. R. Petrescu, A. M. Leach, W. de Vries, *Philos. T. R. Soc. B* **2013**, *368*, 20130116; b) Q. Wang, Y. Guan, J. Guo, P. Chen, *Cell Rep. Phys. Sci.* **2022**, *3*, 100779; c) S. F. McWilliams, D. L. J. Broere, C. J. V. Halliday, S. M. Bhutto, B. Q. Mercado, P. L. Holland, *Nature* **2020**, *584*, 221-226.

[11] a) D. J. Knobloch, E. Lobkovsky, P. J. Chirik, *Nat. Chem.* **2010**, *2*, 30-35; b) K. C. MacLeod, F. S. Menges, S. F. McWilliams, S. M. Craig, B. Q. Mercado, M. A. Johnson, P. L. Holland, *J. Am. Chem. Soc.* **2016**, *138*, 11185-11191.

[12] C. Pattyn, N. Maira, M. Buddhadasa, E. Vervloessem, S. Iseni, N. C. Roy, A. Remy, M. P. Delplancke, N. De Geyter, F. Reniers, *Green Chem.* **2022**, *24*, 7100-7112.

[13] Q. Wang, J. Guo, P. Chen, *Chem* **2021**, *7*, 3203-3220.

[14] a) H. Kirkici, D. Bruno, J. Preiss, G. Schaefer, *J. Appl. Phys.* **1990**, *67*, 6041-6044; b) M. M. Ristić, M. M. Aoneas, M. M. Vojnović, G. B. Poparić, *Plasma Chem. Plasma Process.* **2017**, *37*, 1431-1443.

[15] M. Wang, X.-F. Gao, R. Su, P. He, Y.-Y. Cheng, K. Li, D. Mi, X. Zhang, X. Zhang, H. Chen, R. G. Cooks, *CCS Chem.* **2022**, *3*, 3559-3566.

[16] a) X. Zhang, X. Ren, Y. Zhong, K. Chingin, H. Chen, *Analyst* **2021**, *146*, 5037-5044; b) D. Mi, Y. Mao, B. Wei, Y.-C. Li, X. Dong, K. Chingin, *J. Am. Soc. Mass Spectrom.* **2022**, *33*, 68-73; c) X. Zhang, X. Ren, K. Chingin, J. Xu, X. Yan, H. Chen, *Anal. Chim. Acta* **2020**, *1139*, 146-154.

[17] a) D. Xing, Y. Meng, X. Yuan, S. Jin, X. Song, R. N. Zare, X. Zhang, *Angew. Chem. Int. Ed.* **2022**, *61*, e202207587; b) L. Qiu, N. M. Morato, K.-H. Huang, R. G. Cooks, *Front. Chem.* **2022**, *10*, 903774.

[18] S. W. Sharpe, P. M. Johnson, *J. Chem. Phys.* **1986**, *85*, 4943-4948.

[19] Y. Yao, H. Wang, X.-z. Yuan, H. Li, M. Shao, *ACS Energy Lett.* **2019**, *4*, 1336-1341.

[20] D. S. Frear, R. C. Burrell, *Anal. Chem.* **1955**, *27*, 1664-1665.

[21] G.-J. Mao, X.-B. Zhang, X.-L. Shi, H.-W. Liu, Y.-X. Wu, L.-Y. Zhou, W. Tan, R.-Q. Yu, *Chem. Commun.* **2014**, *50*, 5790-5792.

[22] L. Dal Pozzo, G. Fornasari, T. Monti, *Catal. Commun.* **2002**, *3*, 369-375.

[23] L. F. Zhu, B. Guo, D. Y. Tang, X. K. Hu, G. Y. Li, C. W. Hu, *J. Catal.* **2007**, *245*, 446-455.

[24] X. Deng, G. Zhou, J. Tian, R. Srinivasan, *Angew. Chem. Int. Ed.* **2021**, *60*, 7024-7029.

[25] H. Zhu, Y. Shen, Q. Deng, C. Huang, T. Tu, *Chem. Asian J.* **2017**, *12*, 706-712.

[26] F. Zhao, K. You, C. Peng, S. Tan, R. Li, P. Liu, J. Wu, H. a. Luo, *Chem. Eng. J.* **2015**, *272*, 102-107.

[27] Z. Du, D. Denkenberger, J. M. Pearce, *Sol. Energy* **2015**, *122*, 562-568.

[28] M. R. Walter, S. P. Dzul, A. V. Rodrigues, T. L. Stemmler, J. Telser, J. Conradie, A. Ghosh, T. C. Harrop, *J. Am. Chem. Soc.* **2016**, *138*, 12459-12471.

[29] a) Y. Tian, N. Paolocci, W. D. Gao, *Engineering* **2015**, *1*, 401-404; b) H.-J. Sun, Z.-Y. Wu, L. Cao, M.-Y. Zhu, X.-W. Nie, D.-J. Huang, M.-T. Sun, J.-S. Bian, *Pharmacol. Res.* **2020**, *159*, 104961.

[30] E. M. Shoman, M. O. Aly, *Curr. Top. Med. Chem.* **2016**, *16*, 2464-2470.

[31] J. C. Irvine, R. H. Ritchie, J. L. Favaloro, K. L. Andrews, R. E. Widdop, B. K. Kemp-Harper, *Trends Pharmacol. Sci.* **2008**, *29*, 601-608.

[32] X. Xue, R. Chen, C. Yan, P. Zhao, Y. Hu, W. Zhang, S. Yang, Z. Jin, *Nano Res.* **2019**, *12*, 1229-1249.

[33] X.-D. An, S. Yu, *Org. Lett.* **2015**, *17*, 5064-5067.

Entry for the Table of Contents

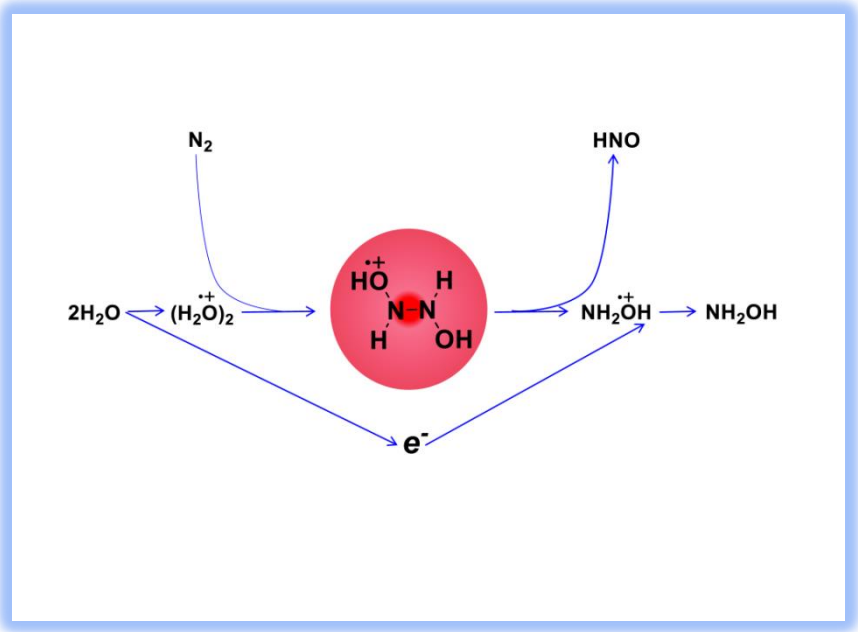

Green N_2 fixation into two high value-added products, HNO and NH_2OH is demonstrated through disproportionation reaction with water dimer radical cations $(H_2O)_2^{+\bullet}$, under mild ambient conditions requiring neither catalyst nor toxic chemicals.